Zsarnoczay et al. European Radiology Experimental (2024)8:102
https://doi.org/10.1186/s41747-024-00482-w

European Radiology EXPERIMENTAL

ORIGINAL ARTICLE Open Access

Accuracy of ultra-high resolution and virtual non-calcium reconstruction algorithm for stenosis evaluation with photon-counting CT: results from a dynamic phantom study

Emese Zsarnoczay[1,2], Nicola Fink[1,3], U. Joseph Schoepf[1], Daniel Pinos[1], Jim O'Doherty[1,4], Thomas Allmendinger[5], Junia Hagenauer[5,6], Joseph P. Griffith III[1], Milán Vecsey-Nagy[1,7], Pál Maurovich-Horvat[2], Tilman Emrich[1,8,9*] and Akos Varga-Szemes[1]

Abstract

Background We compared ultra-high resolution (UHR), standard resolution (SR), and virtual non-calcium (VNCa) reconstruction for coronary artery stenosis evaluation using photon-counting computed tomography (PC-CT).

Methods One vessel phantom (4-mm diameter) containing solid calcified lesions with 25% and 50% stenoses inside a thorax phantom with motion simulation underwent PC-CT using UHR (0.2-mm slice thickness) and SR (0.6-mm slice thickness) at heart rates of 60 beats per minute (bpm), 80 bpm, and 100 bpm. A paired *t*-test or Wilcoxon test with Bonferroni correction was used.

Results For 50% stenosis, differences in percent mean diameter stenosis between UHR and SR at 60 bpm (51.0 vs 60.3), 80 bpm (51.7 vs 59.6), and 100 bpm (53.7 vs 59.0) ($p \leq 0.011$), as well as between VNCa and SR at 60 bpm (50.6 vs 60.3), 80 bpm (51.5 vs 59.6), and 100 bpm (53.7 vs 59.0) were significant ($p \leq 0.011$), while differences between UHR and VNCa at all heart rates ($p \geq 0.327$) were not significant. For 25% stenosis, differences between UHR and SR at 60 bpm (28.0 vs 33.7), 80 bpm (28.4 vs 34.3), and VNCa vs SR at 60 bpm (29.1 vs 33.7) were significant ($p \leq 0.015$), while differences for UHR vs SR at 100 bpm (29.9 vs 34.0), as well as for VNCa vs SR at 80 bpm (30.7 vs 34.3) and 100 bpm (33.1 vs 34.0) were not significant ($p \geq 0.028$).

Conclusion Stenosis quantification accuracy with PC-CT improved using either UHR acquisition or VNCa reconstruction.

Relevance statement PC-CT offers to scan with UHR mode and the reconstruction of VNCa images both of them could provide improved coronary stenosis quantification at increased heart rates, allowing a more accurate stenosis grading at low and high heart rates compared to SR.

*Correspondence:
Tilman Emrich
tilman.emrich@unimedizin-mainz.de
Full list of author information is available at the end of the article

Key Points

- Evaluation of coronary stenosis with conventional CT is challenging at high heart rates.
- PC-CT allows for scanning with ECG-gated UHR and SR modes.
- UHR and VNCa images were compared in a dynamic phantom.
- UHR improves stenosis quantification up to 100 bpm.
- VNCa reconstruction improves stenosis evaluation up to 80 bpm.

Keywords Computed tomography angiography, Coronary stenosis, Heart rate, Phantoms (imaging), Tomography (x-ray computed)

Graphical Abstract

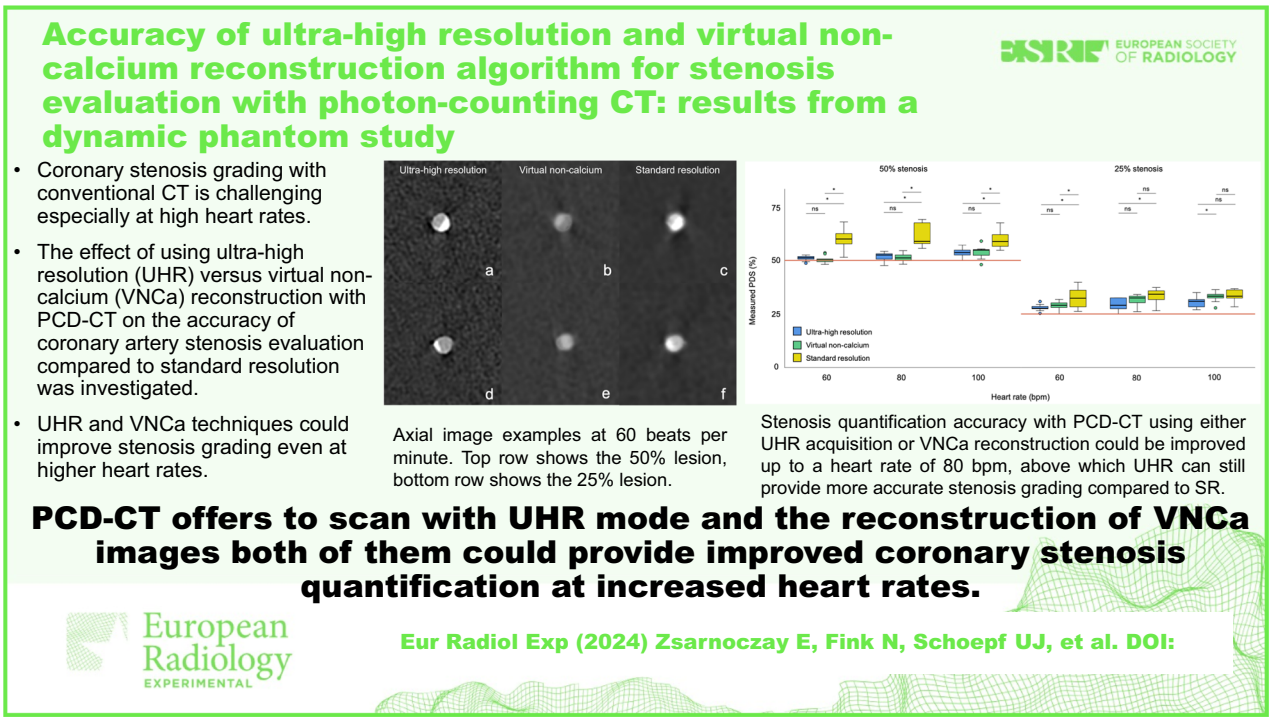

Background

Coronary computed tomography (CT) angiography has emerged as an established noninvasive imaging modality with a class I indication for the evaluation of symptomatic patients with suspected coronary artery disease [1–3]. Extensive evidence has supported its effective role as a gatekeeper to invasive cardiac catheterization, which carries the risk of major complications [4]. However, limitations do exist. For example, the evaluation of the coronary lumen and stenosis severity may be challenging with conventional CT technology, especially in the presence of severe calcifications and/or at higher heart rates [5, 6]. High coronary calcification burden often leads to blooming artifacts causing an overestimation of stenosis grade [7]. As a consequence, the probability of a false-positive diagnosis and the overestimation of stenosis relevance are considerable with conventional techniques [8, 9].

The recently introduced whole-body, dual-source, photon-counting computed tomography (PC-CT) detector uses cadmium telluride crystal semiconductors that directly convert x-ray photons to electronic signals instead of an indirect conversion used by conventional systems [10]. PC detectors count every incident photon equally and determine their associated energy. Furthermore, electronic noise is reduced since only x-rays with an energy over 20 keV are counted by readout electronics [11]. Acquisition at ultra-high resolution (UHR) with conventional CT systems is limited by the detector pixel size which could not be reduced significantly in recent

years. In conventional systems, spatial resolution can be improved by other techniques such as with the use of comb or grid filters, which however reduce radiation dose efficiency. On the other hand, PC-CT allows for UHR scanning with a specific scan mode utilizing a minimum detector pixel size of $0.151 \times 0.176\ mm^2$ at the isocenter while maintaining a high temporal resolution [12, 13]. PC-CT demonstrated the potential to reduce image artifacts and noise, while still improving dose efficiency and contrast-to-noise ratio [14–16].

In addition, the multi-energy capabilities of the PC-CT system make it possible to reconstruct spectral images scanned with standard resolution (SR) (collimation of 144×0.4 mm). Material decomposition and generation of spectrally postprocessed images, e.g., iodine removal with preserved calcification [17, 18] and calcium removal to visualize coronary artery lumen by separating calcium and iodine, are also possible with PC-CT [19]. The virtual non-calcium (VNCa) reconstruction algorithm generates images without calcified lesions while leaving other materials unchanged. This algorithm has been recently investigated by Allmendinger et al. [19] in a phantom study demonstrating good image quality and decreased blooming artifacts when visualizing coronary lumen in the presence of calcification, in comparison with virtual monoenergetic images at an intermediate heart rate. Both UHR acquisition [13, 20] and VNCa reconstruction [19] have been shown to improve the accuracy of stenosis quantification and reduce calcium blooming artifacts; however, it remains unknown which technique should be preferred. Hence, we hypothesized that both VNCa spectral reconstruction and UHR acquisition possible with PC-CT would lead to a similar improvement of stenosis grading compared to conventionally reconstructed images at different heart rates.

The purpose of this study was to assess the impact of using UHR vs VNCa reconstruction on the accuracy of coronary artery stenosis evaluation in comparison to virtual monoenergetic reconstructions acquired at SR with PC-CT. This investigation was conducted using a dynamic motion phantom across varying heart rates.

Methods

Phantom

A custom-built vessel phantom (Quality Assurance in Radiology and Medicine [QRM], Moehrendorf, Germany), with a 4-mm diameter was used. The vessel was constructed as a solid cylinder simulating a mixture of iodinated contrast material and blood, with a CT value of 800 HU at 120 kVp with conventional CT. Two 10-mm-long calcified lesions composed of hydroxyapatite with a concentration of 800 mg/mL were embedded within the vessel, with a CT value of 1100 HU on conventional CT at 120 kVp. These lesions were placed at various angles with a 5-mm intermittent space designed to induce stenosis of 50% and 25% diameter relative to the vessel diameter. An illustration of the vessel phantom is shown in Fig. 1.

In our study, we used an anthropomorphic chest CT phantom (Cardio CT Phantom, QRM, Moehrendorf, Germany) and a three-dimensional coronary motion simulator phantom (Sim4DCardio, QRM). The thorax phantom, measuring $300 \times 200 \times 100$ mm, reproduced the characteristics of an average-sized patient in terms of thoracic tissue density. Inside the thoracic phantom, a 100-mm diameter water tank housed the coronary motion simulator, which was attached to the vascular phantom. The setup of the phantom is shown in Fig. 2. The coronary motion phantom simulated three-dimensional computer-guided motion along the *x*-, *y*-, and *z*-axes with small amplitudes (2 mm in-plane and 3 mm out-of-plane). This

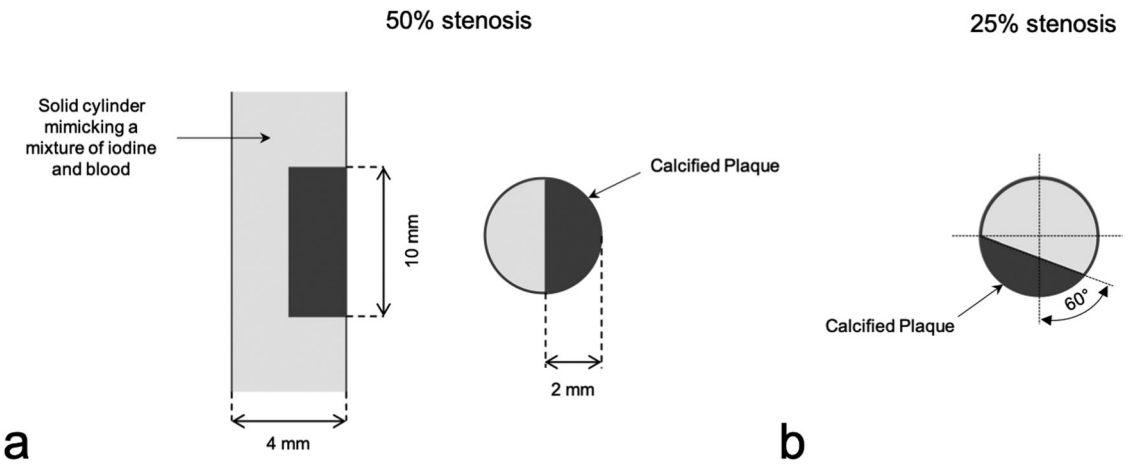

Fig. 1 Longitudinal and cross-sectional drawing of 50% stenosis (**a**) and cross-sectional drawing of 25% stenosis (**b**)

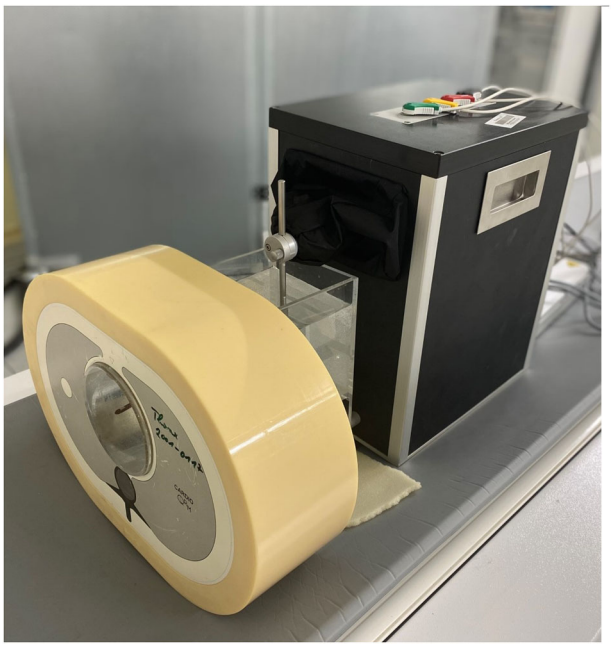

Fig. 2 Image capturing the phantom configuration, comprising the chest phantom and the four-dimensional coronary motion simulator

motion phantom generated an artificial electrocardiogram (ECG) signal, simulating heart rates between 50 beats per minute (bpm) and 100 bpm. The motion profiles determined by the manufacturer were derived from clinical coronary vessel velocity profiles originally obtained from electron beam CT data [21].

Image acquisition and reconstruction

All acquisitions were performed on a whole-body, PC-CT system (NAEOTOM Alpha; Siemens Healthineers, Forchheim, Germany) using an ECG-gated dual-source mode. UHR scans were performed with the following acquisition parameters: tube voltage 120 kVp, collimation 120 × 0.2 mm, gantry rotation time 0.25 s, temporal resolution 66 ms, and ECG pulsing phase at 30–80% of the R-R interval. UHR scans were acquired at heart rates of 60 bpm, 80 bpm, and 100 bpm. In addition to the UHR scans, SR image acquisition was performed with the same parameters, except for a collimation of 144 × 0.4 mm.

At the time of the study, the PC-CT system allows for the collection of ECG-gated spectral information with standard collimation (144 × 0.4 mm), but not with the UHR mode (120 × 0.2 mm). Therefore, virtual monoenergetic images (referred to as SR) and VNCa images were reconstructed from data acquired with standard collimation, while UHR images were reconstructed as a separate set of images (specified as 'T3D' by the manufacturer) from data acquired with a collimation of 120 × 0.2 mm.

Reconstructions of phantom data were performed on a dedicated research workstation using proprietary image reconstruction software (ReconCT, version 15.0.58757.0; Siemens Healthineers). UHR images were post-processed using a Bv64 vascular kernel—according to recommendations by Mergen et al. [13]—in the diastolic phase after the selection of % R–R phase with the least motion artifacts, field of view 150 mm, at slice thickness 0.2 mm, increment 0.2 mm, and quantum iterative reconstruction strength level 3, individually for each scan at heart rates of 60 bpm, 80 bpm, and 100 bpm. SR images were reconstructed as traditional monoenergetic images and as VNCa images (PureLumen, Siemens Healthineers). The SR images were reconstructed using virtual monoenergetic images at 55 keV (clinical standard), with the default vascular kernel Bv40, field of view 150 mm, slice thickness 0.6 mm, increment 0.4 mm, and quantum iterative reconstruction strength level 3; these images served as the reference standard. VNCa images were reconstructed using virtual monoenergetic images at 65 keV (vendor recommendation for VNCa), with a Qr44 kernel, while all other reconstruction parameters were matched to those used for the SR images. The VNCa algorithm used in our study is based on spectrally resolved multi-threshold PC-CT data allowing for reconstruction of images without all contributors from calcium or bone-like materials while leaving other material's attenuation values unchanged. A detailed description of the algorithm can be found in a previous publication by Allmendinger et al. [19].

Quantitative analysis

Quantitative analysis was performed with commercially available software (CT Coronary, Syngo.via, Siemens) on the UHR, VNCa, and SR scans as shown in Fig. 3. The percent diameter stenosis (PDS) was calculated as follows [19]:

$$\mathrm{PDS} = \left[1 - \left(\frac{\mathrm{D_L}}{\mathrm{D_V}}\right)\right] \times 100$$

where D_L represents the minimal lumen diameter measured in cross-sectional images at the site of the lesions, and D_v is the average of the normal vessel lumen diameters proximal and distal to the stenosis. PDS was measured in percentages at each calcified lesion. Window/level settings were set for each reconstruction to the same values (center 450 HU, width 1500 HU).

Quantitative measurements were performed independently by three readers with 4 years, 2 years, and 2 years of experience in cardiovascular imaging, repeating the measurements three consecutive times.

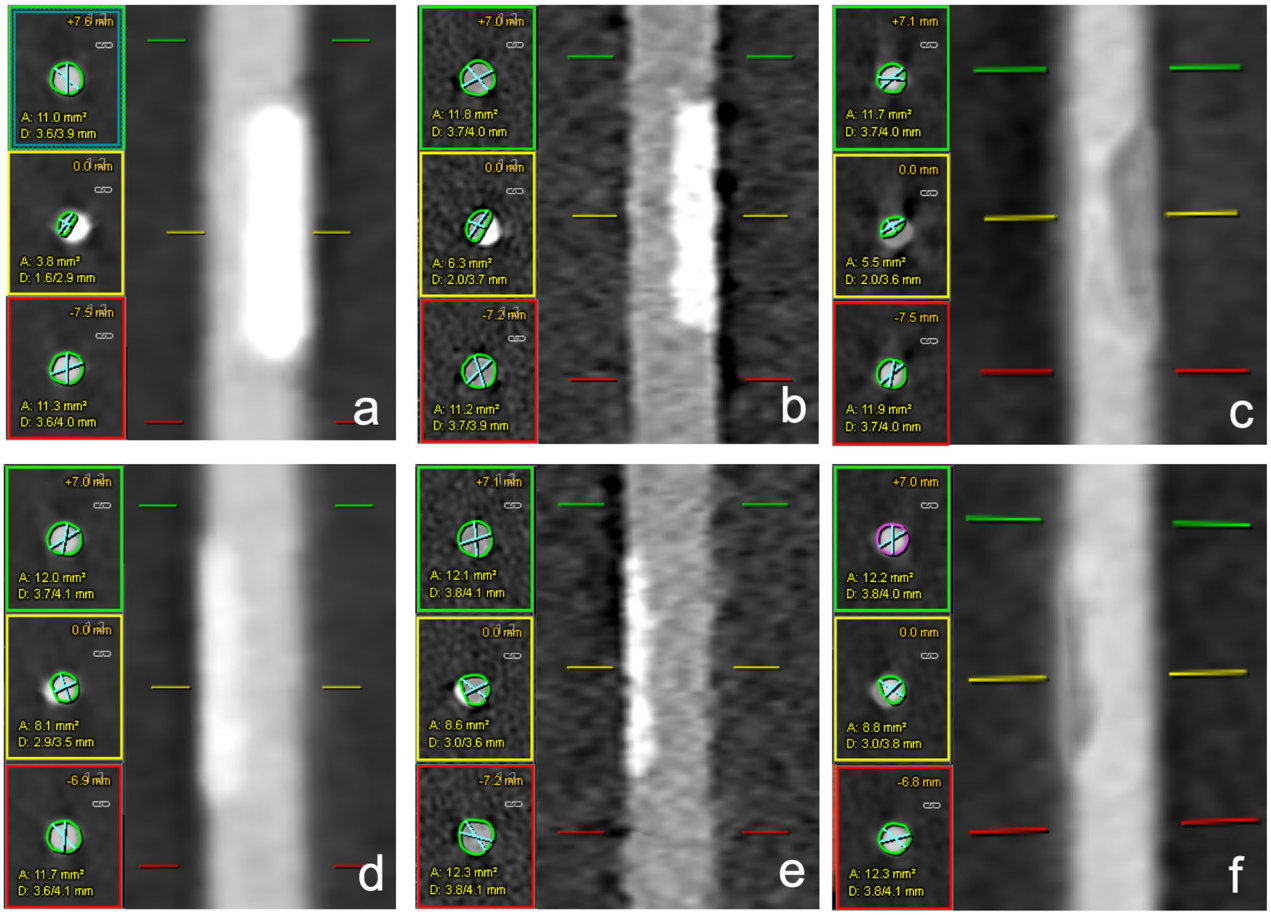

Fig. 3 Example of stenosis quantification for the vessel phantom at 60 bpm for the 50% stenosis with SR (**a**), UHR (**b**), VNCa (**c**), and for the 25% stenosis with SR (**d**), UHR (**e**), and VNCa (**f**) using commercial software (Syngo.via, Siemens Healthineers). Stenosis was identified with markers at the yellow (middle), upper reference at the green (top), and lower reference at the red (bottom) locations. *SR*, standard resolution; *UHR*, ultra-high resolution; *VNCa*, virtual non-calcium

Statistical analysis

Statistical analysis was performed in MedCalc Statistical Software Version 19.2.6 (MedCalc Software Ltd.; Ostend, Belgium) and SPSS Version 28.0.1.0 (IBM; Chicago, IL, USA). Continuous data were tested for normality with the Shapiro-Wilk test. PDS values are reported as mean ± standard deviation if normally distributed, median with interquartile range if non-normally distributed.

The differences in PDS_{SR}, PDS_{UHR}, and PDS_{VNCa} were assessed by box and whisker plots and paired *t*-test or Wilcoxon test, depending on the distribution. Bonferroni correction was applied and a *p*-value of $0.05/3 = 0.017$ was considered significant for testing the three different reconstructions. The agreement was examined both within (intra-reader) and across (inter-reader) readers for all measurements using intraclass correlation coefficient (ICC) with two-way mixed effects and absolute agreement (0.0–0.3, lack of agreement; 0.31–0.5, weak; 0.51–0.7, moderate; 0.71–0.9, strong; and 0.91–1.00, very strong agreement [22]).

Results

The measured PDS values with UHR, VNCa, and SR techniques are reported in Tables 1–3 and Fig. 4. For the 50% stenosis, there was a significant difference between PDS_{UHR} compared to PDS_{SR} at all heart rates, and PDS_{UHR} measurements were closer to the nominal stenosis. The comparison of PDS_{VNCa} and PDS_{SR} values also showed a significant difference for the 50% stenosis at all heart rates with PDS_{VNCa} closer to the actual stenosis size. When comparing values between PDS_{UHR} and PDS_{VNCa} for the 50% lesion, there was no significant difference at any heart rate.

For the 25% lesion, there was a significant difference between PDS_{UHR} compared to PDS_{SR} at 60 bpm and 80 bpm, with PDS_{UHR} measurements closer to the actual lesion size, and there was no difference at 100 bpm. When

Table 1 Comparison of PDS values between SR and UHR techniques

	HR (bpm)	PDS_{SR}	PDS_{UHR}	*p*-value
50% Stenosis	60	60.3 ± 4.9	51.0 ± 1.3	**0.011**
	80	59.6 ± 3.4	51.7 ± 2.2	**0.008**
	100	59.0 ± 2.9	53.7 ± 2.1	**0.011**
	All	59.6 ± 2.6	52.1 ± 2.1	**< 0.001**
25% Stenosis	60	33.7 ± 3.3	28.0 ± 1.6	**0.008**
	80	34.3 ± 1.9	28.4 ± 2.3	**0.015**
	100	34.0 ± 2.1	29.9 ± 2.6	0.028
	All	33.9 ± 2.5	28.8 ± 2.3	**< 0.001**
Overall	All	45.6 [33.3–59.0]	41.3 [28.4–52.5]	**< 0.001**

Values are mean ± standard deviation or median [interquartile range], depending on the distribution. Significant *p*-values after Bonferroni correction in bold characters
bpm, beats per minute; PDS, percent diameter stenosis; *SR*, standard resolution; *UHR*, ultra-high resolution

Table 2 Comparison of PDS values between SR and VNCa techniques

	Heart rate (bpm)	PDS_{SR}	PDS_{VNCa}	*p*-value
50%	60	60.3 ± 4.9	50.6 ± 1.7	**0.011**
Stenosis	80	59.6 ± 3.4	51.5 ± 2.1	**0.008**
	100	59.0 ± 2.9	53.7 ± 3.1	**0.011**
	All	59.6 ± 2.6	51.9 ± 2.6	**< 0.001**
25%	60	33.7 ± 3.3	29.1 ± 2.0	**0.008**
Stenosis	80	34.3 ± 1.9	30.7 ± 2.3	0.110
	100	34.0 ± 2.1	33.1 ± 2.6	0.859
	All	33.9 ± 2.5	30.9 ± 2.8	**< 0.001**
Overall	All	45.6 [33.3–59.0]	42.5 [30.8–51.2]	**< 0.001**

Values are mean ± standard deviation or median [interquartile range], depending on the distribution. Significant *p*-values after Bonferroni correction in bold characters
bpm, beats per minute; *PDS*, percent diameter stenosis; *SR*, standard resolution; *VNCa*, virtual non-calcium

comparing PDS_{VNCa} to PDS_{SR}, there was a significant difference at 60 bpm, with PDS_{VNCa} closer to the actual stenosis size, but there was no difference at 80 bpm and 100 bpm. The comparison of PDS_{UHR} and PDS_{VNCa} measurements showed no significant difference at 60 bpm and 80 bpm. However, the difference was significant at 100 bpm, with PDS_{UHR} measurements closer to the actual stenosis size.

The inter-reader agreement was strong for PDS_{SR} (ICC = 0.90, 95% CI: 0.80–0.96), and very strong for PDS_{UHR} (ICC = 0.97, 95% CI: 0.94–0.99) and for PDS_{VNCa} (ICC = 0.95, 95% CI: 0.89–0.98). Intra-reader agreement was very strong for all three readers (Reader 1: ICC = 0.96, 95% CI: 0.91–0.98; Reader 2: ICC = 0.97, 95% CI: 0.93–0.99; Reader 3: ICC = 0.95, 95% CI: 0.90–0.98).

Table 3 PDS values measured by UHR and VNCa techniques

	Heart rate (bpm)	PDS_{UHR}	PDS_{VNCa}	*p*-value
50%	60	51.0 ± 1.3	50.6 ± 1.7	0.327
Stenosis	80	51.7 ± 2.2	51.5 ± 2.1	0.674
	100	53.7 ± 2.1	53.7 ± 3.1	0.859
	All	52.1 ± 2.1	51.9 ± 2.6	0.619
25%	60	28.0 ± 1.6	29.1 ± 2.0	0.260
Stenosis	80	28.4 ± 2.3	30.7 ± 2.3	0.138
	100	29.9 ± 2.6	33.1 ± 2.6	0.038
	All	28.8 ± 2.3	30.9 ± 2.8	**0.005**
Overall	All	41.3 [28.4–52.5]	42.5 [30.8–51.2]	0.067

Values are mean ± standard deviation or median [interquartile range], depending on the distribution. Significant *p*-values after Bonferroni correction in bold characters
bpm, beats per minute; *PDS*, percent diameter stenosis; *UHR*, ultra-high resolution; *VNCa*, virtual non-calcium

Figure 5 represents sample images of the 50% and 25% lesions at a heart rate of 60 bpm for UHR, VNCa, and SR.

Discussion

This phantom study evaluated the application of UHR acquisition and VNCa reconstruction in comparison to conventional SR acquisition using a PC-CT system in a coronary artery motion phantom. Our results indicate that both the UHR and the VNCa techniques provide improved quantification for 50% stenosis from low to high heart rates when compared to SR. UHR improved the quantification for the small stenosis as well, independent of heart rate, while VNCa maintained its performance for the 25% stenosis up to 80 bpm.

Our study results show that PDS measurements with UHR and VNCa were closer to the nominal stenosis compared to SR. These results resemble a recent publication by Allmendinger et al. [19] in which the VNCa reconstruction performed well in the presence of motion up to a heart rate of 80 bpm. However, in that study, only qualitative analysis was performed for each heart rate, and quantitative evaluation was implemented only in a pooled fashion. In our study, PDS measurements showed consistently closer values to the nominal stenosis with UHR and VNCa for both lesions at all investigated heart rates. Furthermore, all three reconstructions showed strong to very strong ICC, however, UHR and VNCa further improved the inter-reader agreement when compared to SR. Reproducibility was assessed with intra-reader agreement analysis which showed very strong agreement for all three readers. However, it is worth mentioning that our measurements at SR for the 50% stenosis did not show a consistent increase with increasing heart rates. Similar results were reported by a recent study [23]

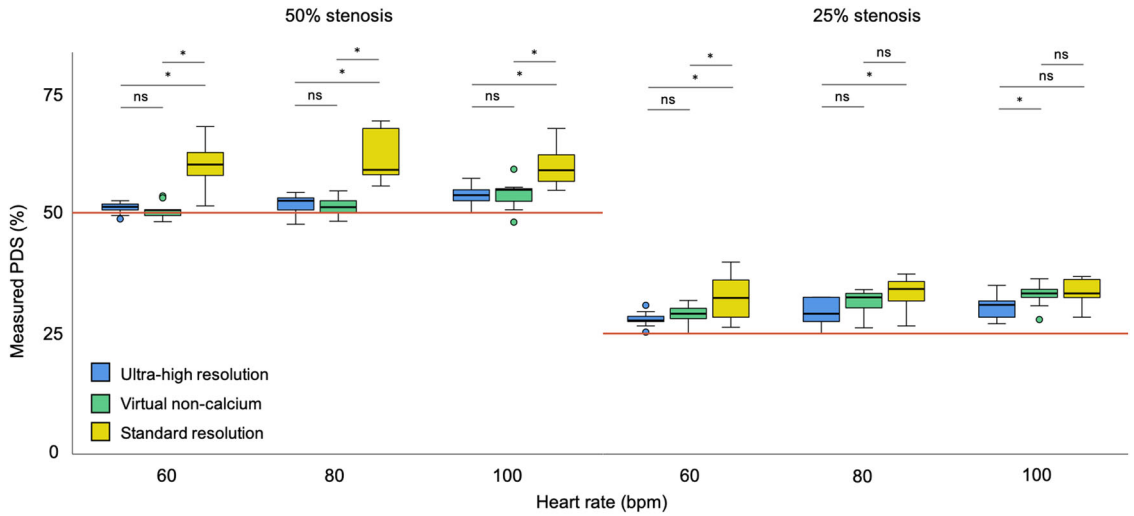

Fig. 4 Comparison of measured PDS values illustrated as paired box and whisker plots for the UHR, VNCa, and SR reconstructions at different heart rates. ns, $p > 0.017$; *$p \leq 0.017$; **$p \leq 0.001$. See the "Methods" section for Bonferroni correction

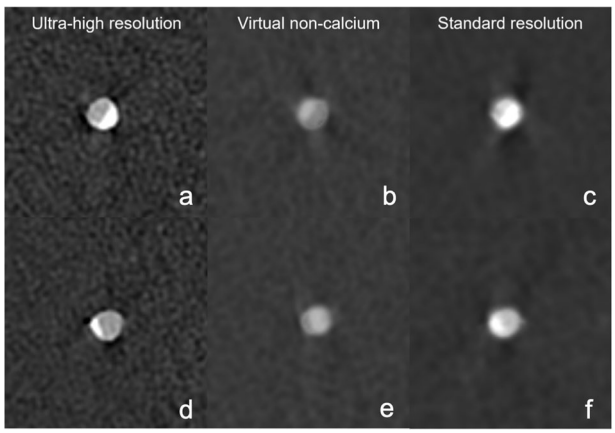

Fig. 5 Axial image examples at 60 bpm. Top row shows the 50% lesion with UHR (**a**), VNCa (**b**), and SR (**c**). The bottom row shows the 25% lesion with UHR (**d**), VNCa (**e**), and SR (**f**) techniques

investigating the stability of spectral results at different heart rates, acquisition modes, and cardiac phases using the same CT system and motion phantom. The authors did not demonstrate a consistent increase in spectral results with increasing heart rates at diastole with virtual monoenergetic reconstructions.

While coronary CT angiography is considered a first-line noninvasive test for the evaluation and management of coronary artery disease [3, 24], stenosis quantification remains a challenge in the presence of severe calcifications mostly due to blooming artifacts. Recent advances, such as UHR acquisition and VNCa reconstruction using PC-CT, however, may address this shortcoming by improving the visualization of coronary plaques and adjacent vessel lumen. Clinically, this has the potential to improve the specific and positive predictive value of coronary CT angiography.

Recent patient and phantom studies investigated prototype and clinical UHR PC-CT (slice thickness of 0.2 mm, 0.25 mm, and 0.275 mm) for coronary imaging and showed promising results over SR PC-CT (0.6 mm) with improved visualization of coronary plaques and stents [25–29]. The feasibility and image quality of the current clinical UHR PC-CT for coronary imaging was first investigated by Mergen et al. [30] in which they determined the optimal reconstruction kernel for patients with high coronary calcium load. They suggested the use of Bv64 as the best kernel for plaque characterization, blooming artifact reduction, and the delineation of coronary artery lumen with UHR [31]. They demonstrated reduced blooming artifacts, high image quality, and high vessel sharpness at UHR (slice thickness of 0.2 mm) in comparison to images reconstructed at SR (0.6 mm). The major limitation of the Mergen et al. [31] study is the lack of a reference standard for stenosis measurement, as invasive coronary angiography was not performed in their investigation. Our study addresses such limitations by having ground truth measurements available as a reference for stenosis quantification. In addition, Koons et al. [32] evaluated the potential of UHR PC-CT in quantifying one-sided and ring-shaped stenosis in comparison to conventional CT using a static vessel phantom. PC-CT was found to be more accurate than conventional CT for all phantom configurations, especially for ring-shaped plaques. While the aforementioned papers demonstrated

the feasibility of PC-CT at UHR for plaque visualization and quantification, its potential for improving stenosis quantification over various heart rates has not been explored.

VNCa algorithm, a possible alternative technique to UHR acquisition with the potential to improve stenosis quantification, has been shown to improve image quality and decrease blooming artifacts in vessel phantoms [19].

As demonstrated in our study, both UHR and VNCa have benefits over SR acquisition for coronary artery stenosis quantification, even at higher heart rates. From a clinical perspective, this holds significant merit, especially in cases where the patient presents for coronary CT angiography with an elevated heart rate, and the administration of beta-blockers is deemed contraindicated. Moreover, the expeditious performance of CT scans becomes advantageous if beta-blocker intervention is reserved exclusively for individuals manifesting markedly elevated heart rates surpassing 80 bpm, facilitating faster patient care. However, the current UHR PC-CT technique has its shortcomings, e.g., the lack of spectral acquisition at UHR, meaning that VNCa reconstruction cannot be performed on UHR data due to current technical limitations. While the SR spectral mode allows for a high pitch acquisition, this is unavailable with UHR acquisition due to the current purposefully limited *z*-axis coverage. As a consequence, sequential or spiral mode needs to be used to obtain a full image using UHR, leading to either higher radiation doses or requiring more steps and longer acquisition time, than by using the spectral mode with standard collimation. However, our present results suggest that the use of SR with VNCa may provide a solution to this. In a clinical setting, there may be patients who would benefit from either VNCa at SR or standard reconstruction at UHR. The decision between the two techniques would likely depend on the heart rate (as UHR performed better > 80 bpm) and age (out of concern of higher radiation dose when using UHR). We posit that an ideal solution would eventually be the combination of UHR acquisition and VNCa reconstruction, which may potentially omit blooming artifacts and improve stenosis quantification to the highest level, further improving the positive predictive value of coronary CT angiography in the diagnosis of coronary artery disease.

Our study has some limitations. First, since this was a phantom experiment, the clinical implications of our results warrant further investigations. Second, different vessel sizes and contrast material concentrations were not evaluated and the vessel phantom used had a diameter of 4 mm, which is usually the diameter of the left main coronary artery. The other coronary arteries usually have a diameter of less than 4 mm, therefore it should be investigated whether our findings are also true for vessels with smaller sizes. Third, only calcified plaques with a given density were available. As a consequence, further plaque types were not evaluated. Fourth, the lesions in the vessel phantom had a clear-cut shape and the size distribution was restricted to 50% and 25%. Thus, further studies should evaluate high-grade and irregularly shaped stenoses. Fifth, only one reconstruction setting was used for image postprocessing. Therefore future research should determine the influence of different reconstruction parameters on the performance of VNCa and UHR acquisition-based stenosis grading. Finally, to enable the widespread implementation of these techniques in clinical practice, future studies are warranted to assess the feasibility of the VNCa algorithm in patients and to provide recommendations in which cases UHR vs VNCa should be used when quantifying coronary artery stenosis.

In conclusion, this motion phantom study demonstrated improved stenosis quantification accuracy with PC-CT using either UHR acquisition or VNCa reconstruction techniques even at high heart rates compared to SR.

Abbreviations

bpm	Beats per minute
CT	Computed tomography
ECG	Electrocardiogram
ICC	Intraclass correlation coefficient
PC-CT	Photon-counting CT
PDS	Percent diameter stenosis
SR	Standard resolution
UHR	Ultra-high resolution
VNCa	Virtual non-calcium

Acknowledgements

LLMs were not used for this manuscript. This article belongs to the thematic series entitled "Photon-counting CT: a disrupting innovation in medical imaging" (Guest Editors: Tilman Emrich (Mainz/Germany) and Akos Varga-Szemes (Charleston/US)).

Author contributions

All authors contributed significantly to the manuscript: EZ performed data curation, analysis, and interpretation and drafted the manuscript. UJS supervised the study conception and data interpretation and substantially edited the manuscript. NF, DP, and JPG performed data analysis and substantially revised the manuscript. JOD advised data reconstruction and edited/revised the manuscript. TA and JH performed data curation and revised the manuscript. PMH and MVN revised the manuscript. TE and AVS designed the study, interpreted the study data, and substantially edited the manuscript.

Funding

This study was supported by Siemens Healthineers. Supported by the ÚNKP-23-3-I New National Excellence Program of the Ministry for Culture and Innovation from the source of the National Research, Development and Innovation Fund. Open Access funding enabled and organized by Projekt DEAL.

Data availability

The datasets used and/or analyzed during the current study are available from the corresponding author on reasonable request.

Declarations

Ethics approval and consent to participate
Not applicable.

Consent for publication
Not applicable.

Competing interests
UJS receives institutional research support and/or personal fees from Bayer, Bracco, Elucid Bioimaging, Guerbet, HeartFlow, Inc., Keya Medical, and Siemens. JOD is an employee of Siemens Medical Solutions USA Inc. TA and JH are employees of Siemens Healthcare GmbH. TE received a speaker fee and travel support from Siemens Medical Solutions USA Inc. and institutional research support from Siemens Healthineers. AVS receives institutional research support and/or personal fees from Bayer, Elucid Bioimaging, and Siemens. AVS is a deputy editor and TE is a member of the Scientific Editorial Board (section editor: CT) for European Radiology Experimental, they have not participated in the selection nor review processes for this article. The remaining authors declare no conflicts of interest.

Author details
[1]Division of Cardiovascular Imaging, Department of Radiology and Radiological Science, Medical University of South Carolina, Charleston, SC, USA. [2]MTA-SE Cardiovascular Imaging Research Group, Medical Imaging Centre, Semmelweis University, Budapest, Hungary. [3]Department of Radiology, University Hospital, LMU Munich, Munich, Germany. [4]Siemens Medical Solutions USA Inc, Malvern, PA, USA. [5]Siemens Healthcare GmbH, Forchheim, Germany. [6]Faculty of Medicine, Friedrich Alexander University of Erlangen-Nuremberg, Erlangen, Germany. [7]Cardiovascular Imaging Research Group, Heart and Vascular Center, Semmelweis University, Budapest, Hungary. [8]Department of Diagnostic and Interventional Radiology, University Medical Center of the Johannes Gutenberg-University, Mainz, Germany. [9]German Centre for Cardiovascular Research, Partner site Rhine-Main, Mainz, Germany.

Received: 25 September 2023 Accepted: 26 February 2024
Published online: 29 August 2024

References
1. Haase R, Schlattmann P, Gueret P et al. (2019) Diagnosis of obstructive coronary artery disease using computed tomography angiography in patients with stable chest pain depending on clinical probability and in clinically important subgroups: meta-analysis of individual patient data. BMJ 365:l1945. https://doi.org/10.1136/bmj.l1945
2. Knuuti J, Ballo H, Juarez-Orozco LE et al. (2018) The performance of non-invasive tests to rule-in and rule-out significant coronary artery stenosis in patients with stable angina: a meta-analysis focused on post-test disease probability. Eur Heart J 39:3322–3330. https://doi.org/10.1093/eurheartj/ehy267
3. Knuuti J, Wijns W, Saraste A et al. (2019) 2019 ESC guidelines for the diagnosis and management of chronic coronary syndromes: The Task Force for the diagnosis and management of chronic coronary syndromes of the European Society of Cardiology (ESC). Eur Heart J 41:407–477. https://doi.org/10.1093/eurheartj/ehz425
4. Van Mieghem CAG (2017) CT as gatekeeper of invasive coronary angiography in patients with suspected CAD. Cardiovasc Diagn Ther 7:189–195. https://doi.org/10.21037/cdt.2017.04.03
5. Achenbach S, Moshage W, Ropers D, Nossen J, Daniel WG (1998) Value of electron-beam computed tomography for the noninvasive detection of high-grade coronary-artery stenoses and occlusions. N Engl J Med 339:1964–1971. https://doi.org/10.1056/nejm199812313392702
6. Reddy GP, Chernoff DM, Adams JR, Higgins CB (1998) Coronary artery stenoses: assessment with contrast-enhanced electron-beam CT and axial reconstructions. Radiology 208:167–172. https://doi.org/10.1148/radiology.208.1.9646809
7. Song YB, Arbab-Zadeh A, Matheson MB et al. (2019) Contemporary discrepancies of stenosis assessment by computed tomography and invasive coronary angiography. Circ Cardiovasc Imaging 12:e007720. https://doi.org/10.1161/circimaging.118.007720
8. Vavere AL, Arbab-Zadeh A, Rochitte CE et al. (2011) Coronary artery stenoses: accuracy of 64-detector row CT angiography in segments with mild, moderate, or severe calcification–a subanalysis of the CORE-64 trial. Radiology 261:100–108. https://doi.org/10.1148/radiol.11110537
9. Zhang S, Levin DC, Halpern EJ, Fischman D, Savage M, Walinsky P (2008) Accuracy of MDCT in assessing the degree of stenosis caused by calcified coronary artery plaques. AJR Am J Roentgenol 191:1676–1683. https://doi.org/10.2214/ajr.07.4026
10. Leng S, Bruesewitz M, Tao S et al. (2019) Photon-counting detector CT: system design and clinical applications of an emerging technology. Radiographics 39:729–743. https://doi.org/10.1148/rg.2019180115
11. Flohr T, Schmidt B (2023) Technical basics and clinical benefits of photon-counting CT. Invest Radiol 58:441–450. https://doi.org/10.1097/rli.0000000000000980
12. Benson JC, Rajendran K, Lane JI et al. (2022) A new frontier in temporal bone imaging: photon-counting detector ct demonstrates superior visualization of critical anatomic structures at reduced radiation dose. Am J Neuroradiol 43:579–584. https://doi.org/10.3174/ajnr.A7452
13. Mergen V, Sartoretti T, Baer-Beck M et al. (2022) Ultra-high-resolution coronary CT angiography with photon-counting detector CT: feasibility and image characterization. Invest Radiol. https://doi.org/10.1097/rli.0000000000000897
14. Schwartz FR, Daubert MA, Molvin L et al. (2023) Coronary artery calcium evaluation using new generation photon-counting computed tomography yields lower radiation dose compared with standard computed tomography. J Thorac Imaging 38:44–45. https://doi.org/10.1097/rti.0000000000000685
15. Farhadi F, Rajagopal JR, Nikpanah M et al. (2021) Review of technical advancements and clinical applications of photon-counting computed tomography in imaging of the thorax. J Thorac Imaging 36:84–94. https://doi.org/10.1097/rti.0000000000000569
16. Graafen D, Emrich T, Halfmann MC et al. (2022) Dose reduction and image quality in photon-counting detector high-resolution computed tomography of the chest: routine clinical data. J Thorac Imaging 37:315–322. https://doi.org/10.1097/rti.0000000000000661
17. Emrich T, Aquino G, Schoepf UJ et al. (2022) Coronary computed tomography angiography-based calcium scoring: in vitro and in vivo validation of a novel virtual noniodine reconstruction algorithm on a clinical, first-generation dual-source photon counting-detector system. Invest Radiol 57:536–543. https://doi.org/10.1097/rli.0000000000000868
18. Fink N, Zsarnoczay E, Schoepf UJ et al. (2023) Photon counting detector CT-based virtual noniodine reconstruction algorithm for in vitro and in vivo coronary artery calcium scoring: impact of virtual monoenergetic and quantum iterative reconstructions. Invest Radiol. https://doi.org/10.1097/rli.0000000000000959
19. Allmendinger T, Nowak T, Flohr T et al. (2022) Photon-counting detector ct-based vascular calcium removal algorithm: assessment using a cardiac motion phantom. Invest Radiol 57:399–405. https://doi.org/10.1097/rli.0000000000000853
20. Zsarnoczay E, Fink N, Schoepf UJ et al. (2023) Ultra-high resolution photon-counting coronary CT angiography improves coronary stenosis quantification over a wide range of heart rates—a dynamic phantom study. Eur J Radiol 161:110746. https://doi.org/10.1016/j.ejrad.2023.110746
21. Achenbach S, Ropers D, Holle J, Muschiol G, Daniel WG, Moshage W (2000) In-plane coronary arterial motion velocity: measurement with electron-beam CT. Radiology 216:457–463. https://doi.org/10.1148/radiology.216.2.r00au19457
22. Koo TK, Li MY (2016) A guideline of selecting and reporting intraclass correlation coefficients for reliability research. J Chiropr Med 15:155–163. https://doi.org/10.1016/j.jcm.2016.02.012
23. Liu LP, Shapira N, Sahbaee P et al. (2023) Consistency of spectral results in cardiac dual-source photon-counting CT. Sci Rep 13:14895. https://doi.org/10.1038/s41598-023-41969-7
24. Newby DE, Adamson PD, Berry C et al. (2018) Coronary CT angiography and 5-year risk of myocardial infarction. N Engl J Med 379:924–933. https://doi.org/10.1056/NEJMoa1805971
25. Boccalini S, Si-Mohamed SA, Lacombe H et al. (2022) First in-human results of computed tomography angiography for coronary stent

assessment with a spectral photon counting computed tomography. Invest Radiol 57:212–221. https://doi.org/10.1097/rli.0000000000000835
26. Si-Mohamed SA, Boccalini S, Lacombe H et al. (2022) Coronary CT angiography with photon-counting CT: First-In-Human Results. Radiology 303:303–313. https://doi.org/10.1148/radiol.211780
27. von Spiczak J, Mannil M, Peters B et al. (2018) Photon counting computed tomography with dedicated sharp convolution kernels: tapping the potential of a new technology for stent imaging. Invest Radiol 53:486–494. https://doi.org/10.1097/rli.0000000000000485
28. Rajagopal JR, Farhadi F, Richards T et al. (2021) Evaluation of coronary plaques and stents with conventional and photon-counting CT: benefits of high-resolution photon-counting CT. Radiol Cardiothorac Imaging 3:e210102. https://doi.org/10.1148/ryct.2021210102
29. Decker JA, O'Doherty J, Schoepf UJ et al. (2022) Stent imaging on a clinical dual-source photon-counting detector CT system—impact of luminal attenuation and sharp kernels on lumen visibility. Eur Radiol. https://doi.org/10.1007/s00330-022-09283-4
30. Mergen V, Sartoretti T, Baer-Beck M et al. (2022) Ultra-high-resolution coronary CT angiography with photon-counting detector CT: feasibility and image characterization. Invest Radiol 57:780–788. https://doi.org/10.1097/rli.0000000000000897
31. Mergen V, Eberhard M, Manka R, Euler A, Alkadhi H (2022) First in-human quantitative plaque characterization with ultra-high resolution coronary photon-counting CT angiography. Front Cardiovasc Med 9:981012. https://doi.org/10.3389/fcvm.2022.981012
32. Koons E, VanMeter P, Rajendran K, Yu L, McCollough C, Leng S (2022) Improved quantification of coronary artery luminal stenosis in the presence of heavy calcifications using photon-counting detector CT. Proc SPIE Int Soc Opt Eng 12031:120311A. https://doi.org/10.1117/12.2613019

Publisher's Note